Supporting Information

Ryder et al. 10.1073/pnas.1217470110

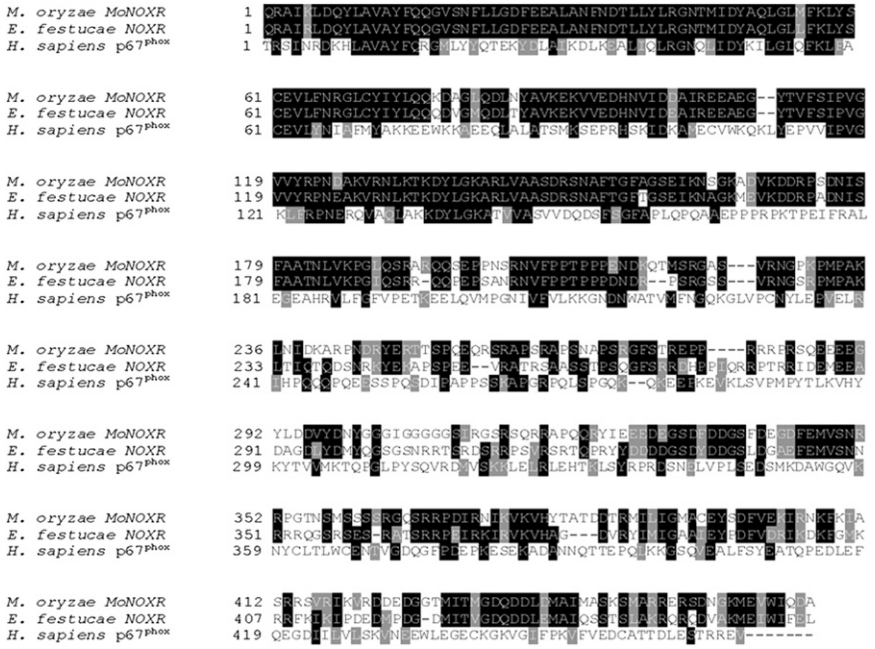

Fig. S1. Amino acid sequence alignment of *M. oryzae* NADPH oxidase isoform R protein. The amino acid sequence of NoxR was aligned with human $p67^{phox}$ and *E. festucae* NoxR. Sequences were aligned using ClustalW and shaded using GeneDoc version 2.6.02. Amino acid residues within a black background were identical among all listed proteins, dark gray residues were identical in two out of three of the listed proteins, and those shown on a white background do not show any similarity.

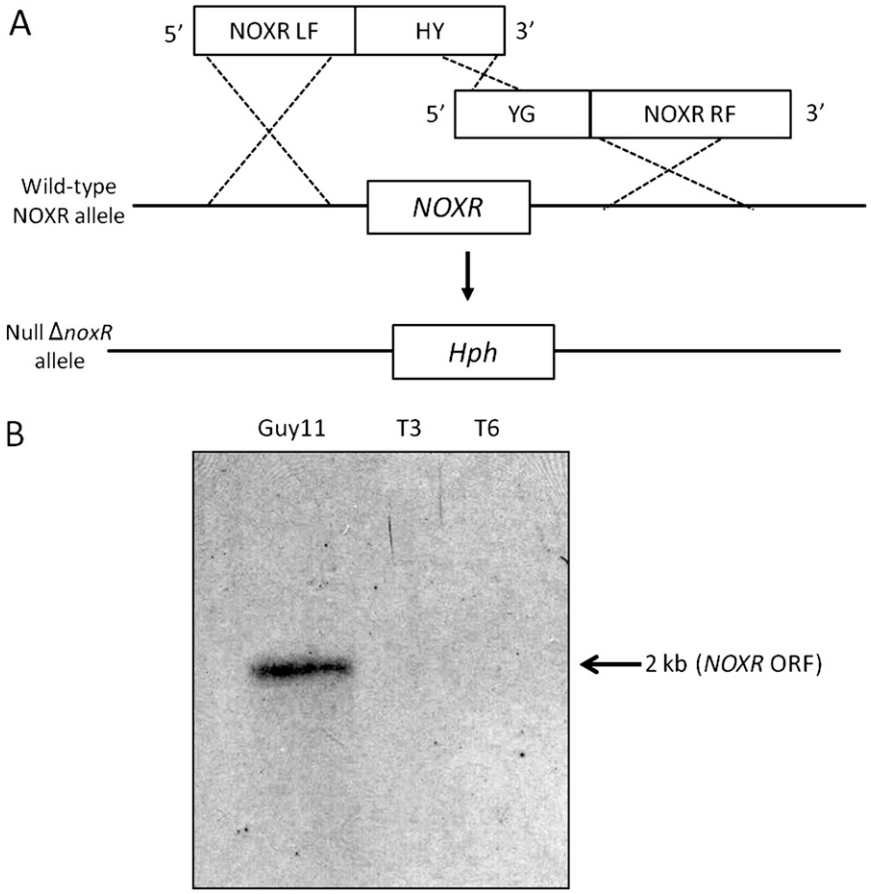

Fig. S2. One-step targeted gene replacement of the *M. oryzae NOXR* gene. (*A*) A 1.4-kb hygromycin B resistance gene cassette was introduced into the NOXR coding sequence using the split marker method. (*B*) Second-round PCR fragments were introduced into *M. oryzae* Guy11 and targeted deletion mutants selected on hygromycin B and identified by probing with a deleted 500-bp region of the *NOXR* coding sequence. Southern blot analysis was carried out and two putative gene replacement mutants, T3 and T6, were identified.

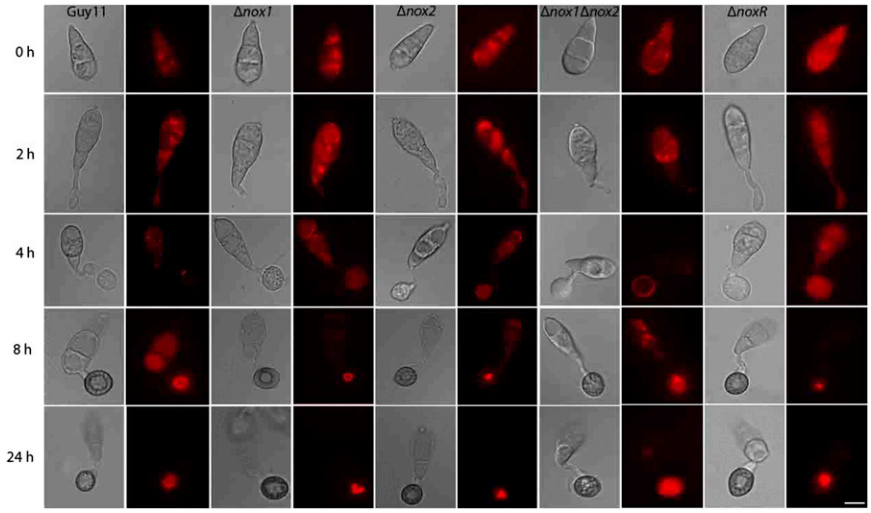

Fig. S3. LifeAct-RFP localization in NADPH oxidase mutants of *M. oryzae*. Micrographs showing expression of LifeAct-RFP in NADPH oxidase mutants during a time course of appressorium development by *M. oryzae*. Conidia were harvested from Guy11, Δ*nox1*, Δ*nox2*, Δ*nox1*Δ*nox2*, and Δ*noxR* mutants expressing LifeAct-RFP, inoculated onto hydrophobic glass coverslips, and observed by epifluorescence microscopy. A toroidal F-actin network was observed in wild-type (Guy11) infection cells at the appressorium pore after 8 h. At 24 h the F-actin network was fully formed and individual actin cables could be distinguished. In Δ*nox1* mutants the F-actin network was distorted and by 24 h the ring-shaped structure at the appressorium pore was no longer intact. In Δ*nox2*, Δ*noxR*, and Δ*nox1* Δ*nox2* mutants the F-actin network was not observed. Instead, a disorganized accumulation of actin was detected in the center of the appressorium. (Scale bar, 10 μm.)

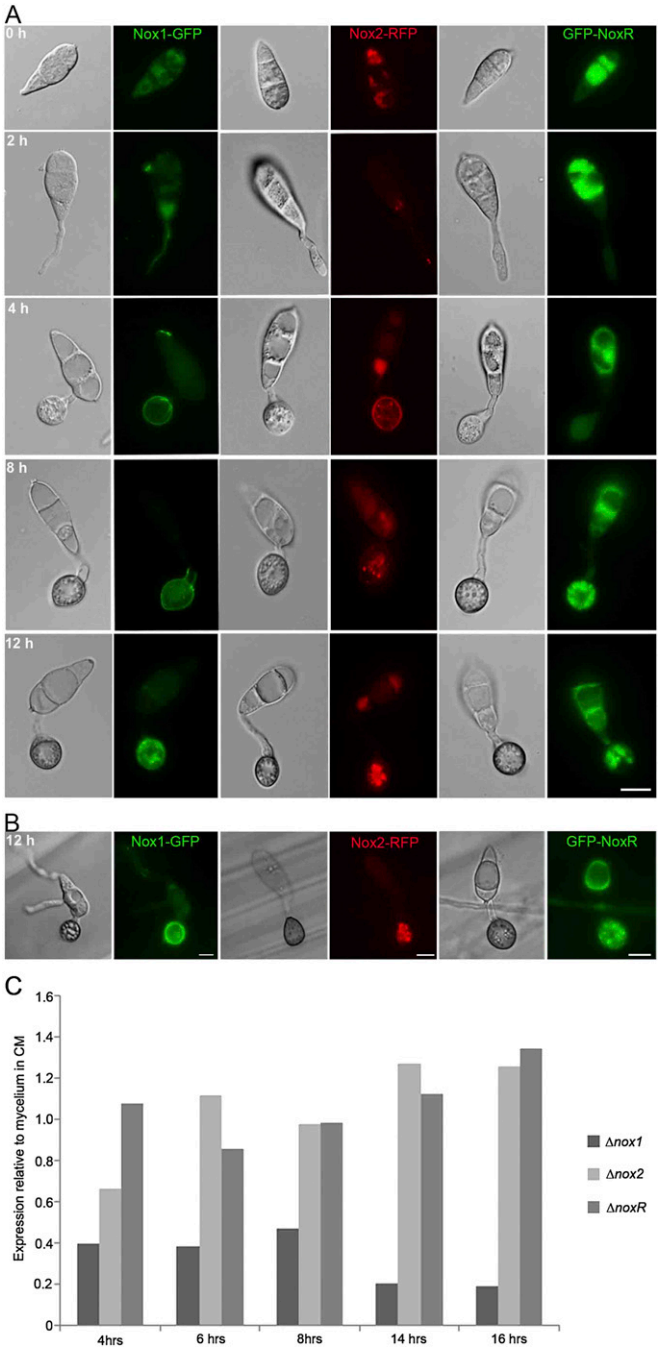

Fig. S4. Live-cell imaging of Nox1-GFP, Nox2-RFP, and GFP-NoxR expressed during appressorium development by *M. oryzae*. Independent transformants were generated expressing *NOX1-GFP, NOX2-RFP*, and *GFP-NOXR* translational gene fusions expressed under control of their native promoters. Strains were inoculated onto hydrophobic glass coverslips and observed by epifluorescence microscopy. (*A*) Nox1-GFP was initially observed at the appressorium cortex from 4 h. After 12 h Nox1-GFP was also observed in the central appressorium vacuole. Nox2-RFP was initially observed at the periphery of the appressorium from 4 h. After 12 h, Nox2-RFP expression increased, forming punctate structures throughout the appressorium. GFP-NoxR expression was observed in the cytoplasm of both ungerminated condia and appressoria. (Scale bar, 10 μm.) (*B*) On a yielding surface that could be ruptured by *M. oryzae* appressoria, similar localization patterns were observed. Conidial suspensions were inoculated onto sterile onion epidermis and observed for a 12-h period. (Scale bar, 10 μm.) (*C*) SuperSAGE analysis showing the expression of Nox genes in Guy11. Bar graphs show abundance of transcripts encoding each Nox gene in a Guy11 time course during appressorium development (4, 6, 8, 14, and 16 h).

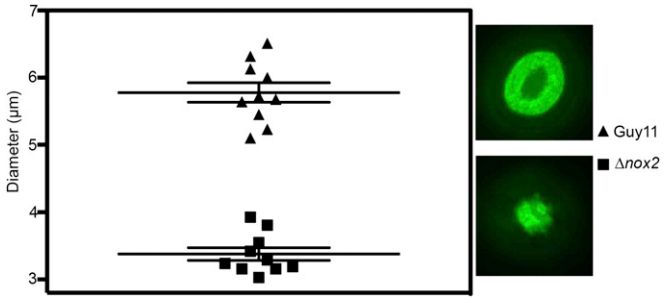

Fig. S5. Graph to show the range of Sep5-GFP ring sizes observed in wild-type and Δ*nox2* mutants of *M. oryzae* during appressorium development. Live-cell imaging experiments were carried out by expression of *SEP5-GFP* in Guy11 or Δ*nox2* mutant. Triangles represent the diameter values of septin rings observed in Guy11. The black squares represent the diameter values of aberrant septin accumulations observed in the Δ*nox2* mutant. Long horizontal lines represent the mean diameter and short horizontal lines are the SEM. The *y* axis shows diameter in micrometers.

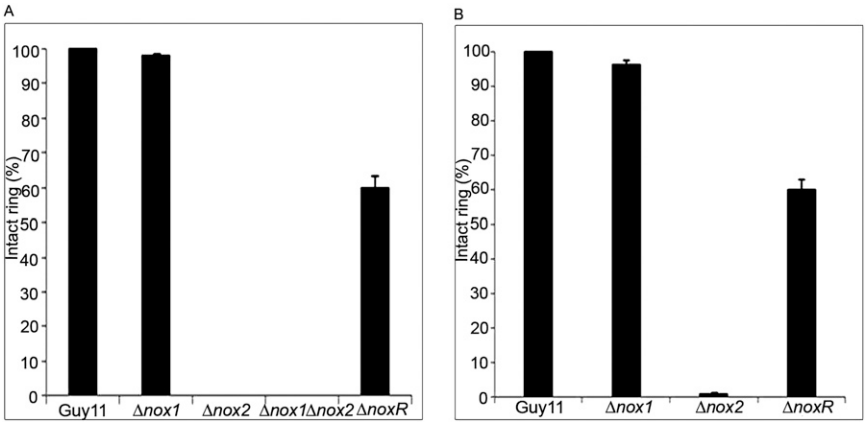

Fig. S6. Live-cell imaging of Sep5-GFP and Chm1-GFP in Δ*nox2* and Δ*noxR* mutants. (*A*) Bar chart showing the percentage of appressoria with intact Sep5-GFP rings after 24 h. Values are mean ±2 SE for three repetitions of the experiment, $n = 100$. (*B*) Bar chart to show the percentage of appressoria containing intact Chm1-GFP rings after 24 h. Values are mean ±2 SE for three repetitions of the experiment, $n = 100$.

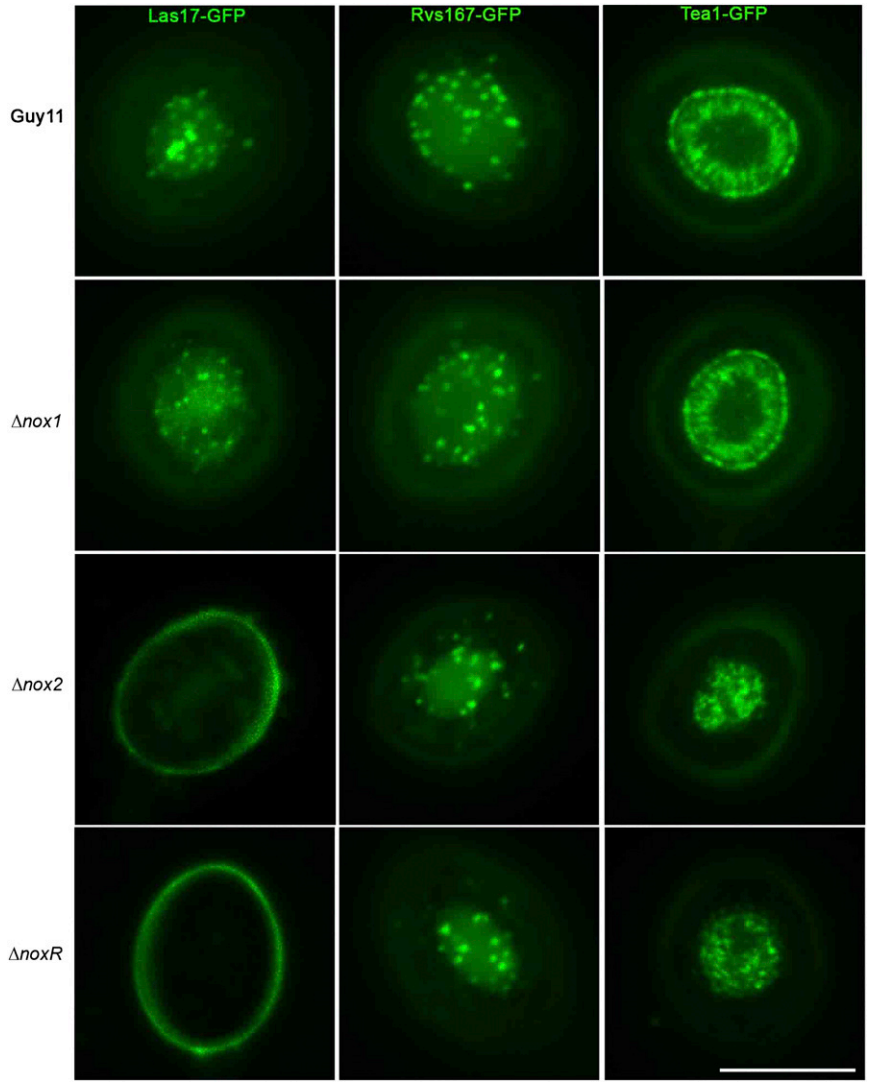

Fig. S7. Expression and localization of Las17-GFP, Tea1-GFP, and Rvs167-GFP in Δ*nox2* and Δ*noxR* mutants of *M. oryzae*. Δ*nox1,* Δ*nox2*, and Δ*noxR* mutants were independently transformed with *LAS17-GFP, TEA1-GFP*, and *RVS167-GFP* gene fusions, inoculated onto glass coverslips, and observed by epifluorescence microscopy. In Δ*nox1* mutants, *Las17-GFP, Tea1-GFP*, and *Rvs167-GFP* localized in the same pattern as Guy11. In Δ*nox2* and Δ*noxR* mutants, *Las17-GFP, Tea1-GFP*, and *Rvs167-GFP* were mislocalized. Therefore, ERM–actin interactions at the appressorium pore, which are essential for linking cortical F-actin to the membrane to facilitate penetration peg emergence, require the Nox2/NoxR complex. (Scale bar, 10 μm.)

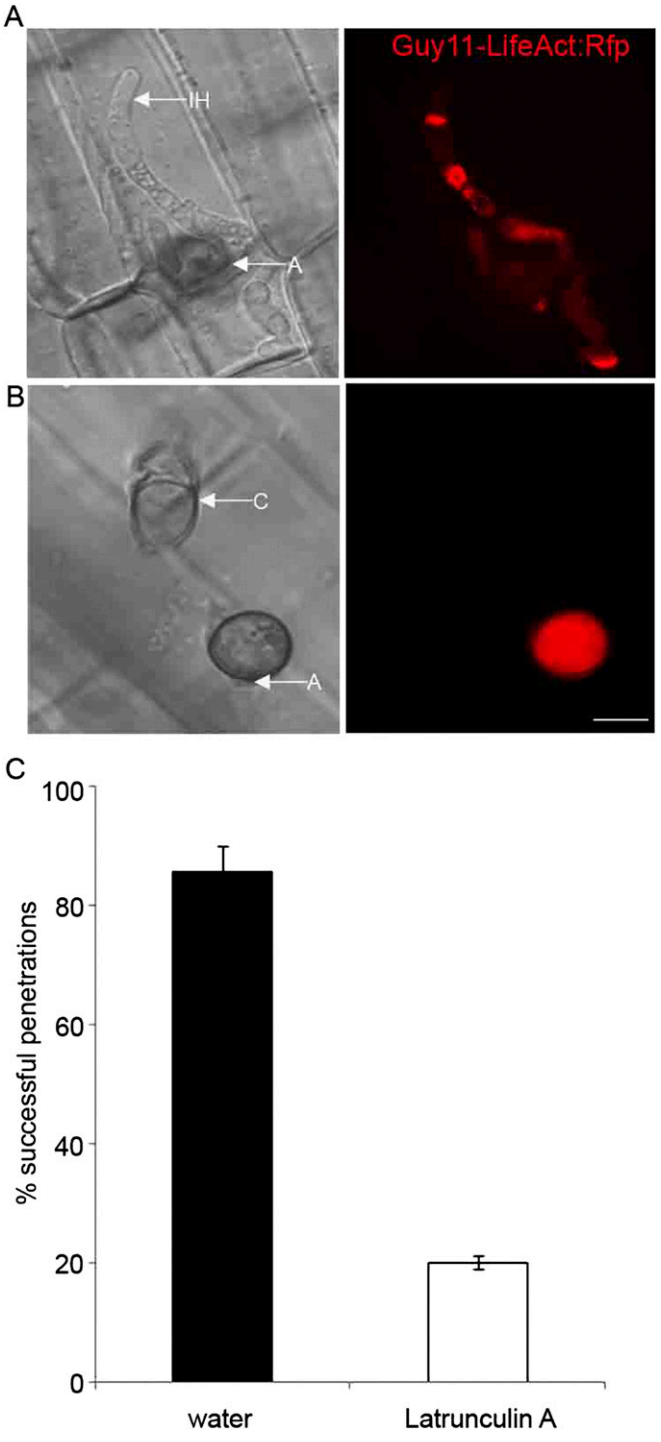

Fig. S8. Exposure to latrunculin A prevents appressorium-mediated rice infection by *M. oryzae*. Micrographs of LifeAct-RFP localization in the presence or absence of latrunculin A. A conidial suspension of the Guy11 expressing LifeAct:RFP at 5×10^4 mL^{-1} was inoculated onto the surface of rice leaf sheath and incubated in a moist chamber at 24 °C. (*A*) Deionized water or (*B*) 3 μg/mL latrunculin A was added to the conidial suspension after 16 h. Representative images were recorded using an IX-81 Olympus inverted microscope. A, appressorium; C, conidium; IH, invasive hypha. (Scale bar, 10 μm.) (*C*) Bar charts to show percentage of appressoria forming penetration pegs after 24 h ($n = 100$). The percentage of appressoria forming penetration hyphae following latrunculin A treatment was significantly reduced ($P < 0.001$) compared with water treatment. Values in *C* are means ±2 SE for three repetitions of the experiment.

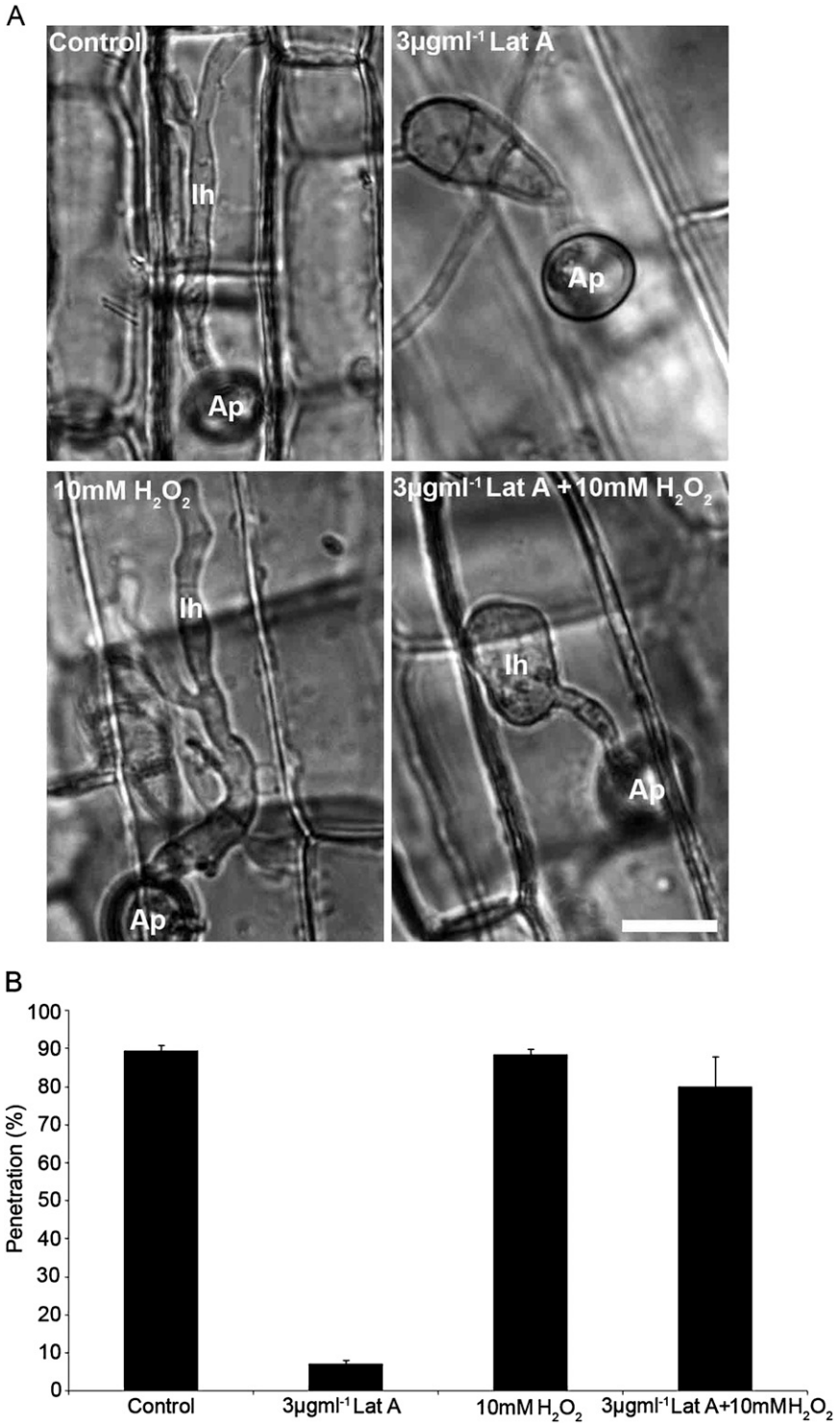

Fig. S9. Addition of H_2O_2 partially remediates the effects of latrunculin A on appressorium-mediated plant infection by *M. oryzae*. A conidial suspension of wild-type Guy11 at 5×10^4 mL^{-1} was inoculated onto the surface of rice leaf sheath and incubated in a moist chamber at 24 °C to form appressoria. At 16 h, deionized water, 3 μg/mL latrunculin A, 10 mM H_2O_2, or 3 μg/mL latrunculin A and 10 mM H_2O_2 was added to the developing appressoria. (*A*) Bright-field micrographs were recorded using an IX-81 Olympus inverted microscope. Ap, appressorium; Ih, invasive hypha. (Scale bar, 10 μm.) (*B*) Bar charts to show percentage of appressoria forming penetration pegs after 24 h ($n = 100$). A significant reduction in penetration peg formation was observed following latrunculin A treatment ($P < 0.001$) but simultaneous addition of 10 mM H_2O_2 restored the frequency of peg formation to almost wild-type levels. Pegs ruptured the leaf cuticle but did not develop into extensive invasion hyphae. Values are means ± 2 SE.

Table S1. Primers used in this study

Primer name	DNA sequence (5′–3′)
NoxR50.1F	GGACGCTACACCCAGCTCCAACAT
NoxR50.1R	GTCGTGACTGGGAAAACCCTGGCGGCTAAAATCAATCAACTCTCTTTT
NoxR30.1F	TTATTCCCTGCTGAGACTTTCATC
NoxR30.1R	TCCTGTGTGAAATTGTTATCCGCTTAAAGCGAGCGATGGTTTTGACTT
Nox2-RFPF	CTGTTACTTTTTTCTGTTACTGTTGTCGCTAATGATCTTGAGTTATTTGGCACT
Nox2-RFPR	TTTGATGACCTCCTCGCCCTTGCTCACCATGAAATTCTCCTTGCCCCATACGAA
NoxRpromF	CTGTTACTTTTTTCTGTTACTGTTGTCGCTCTGGCTCAGCGCCACGAAAA
NoxRpromR	GCTAAAATCAATCAACTCTCTTTT
GFPF	CTAACCAAAAGAGAGTTGATTGATTTTAGCATGGTGAGCAAGGGCGAGGAGCTG
GFPR	CTTGTACAGCTCGTCCATGCCGTG
NoxRORFF	CACGGCATGGACGAGCTGTACAAGTCGCTCAAGCAGGTACGTTCGTTATTCGTA
NoxRORFR	TTCACACAGGAAACAGCTATGACCATGATTGGATGGATATGTTATTTCGGTAG
Gelsolin-GFPF	CTGTTACTTTTTTCTGTTACTGTTGTCGCTACGTTATTCAACACAAACCCACCC
Gelsolin-GFPR	GGTGAACAGCTCCTCGCCCTTGCTCACCATATGGGCTTGAAGCGCCCTCATGAA

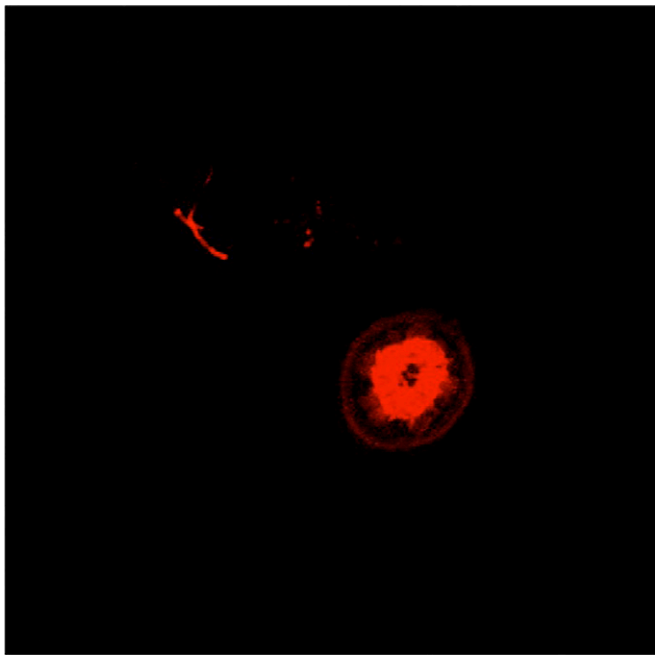

Movie S1. Three-dimensional rotational movie to show toroidal F-actin network at the appressorium pore in the wild-type *M. oryzae* strain Guy11.

Movie S1

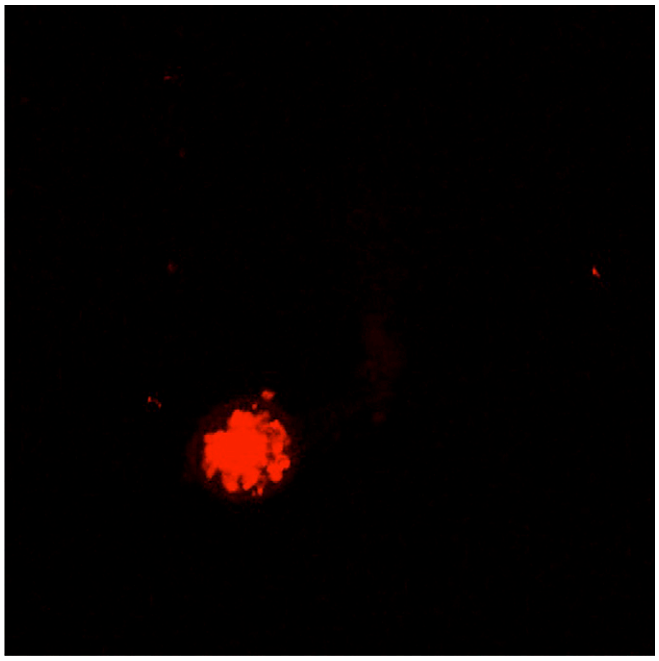

Movie S2. Three-dimensional rotational movie to show misshapen F-actin network at the appressorium pore of the *M. oryzae* Δ*nox1* mutant.

Movie S2

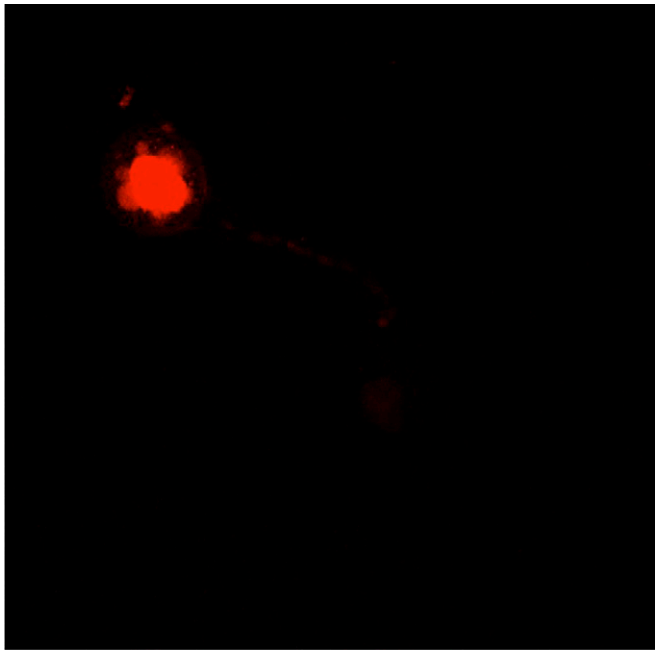

Movie S3. Three-dimensional rotational movie to show distorted F-actin network in the appressorium of the *M. oryzae* Δ*nox2* mutant.

Movie S3

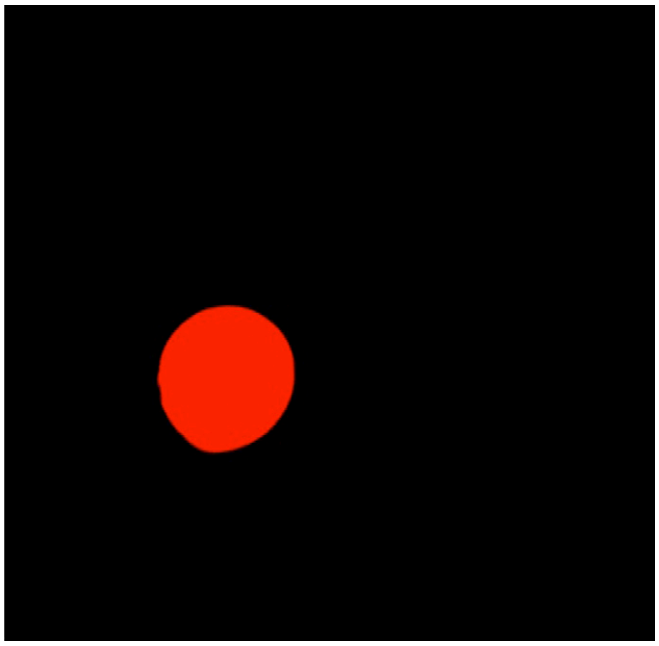

Movie S4. Three-dimensional rotational movie to show distorted F-actin network in the appressorium of the *M. oryzae* Δ*nox1*Δ*nox2* mutant.

Movie S4

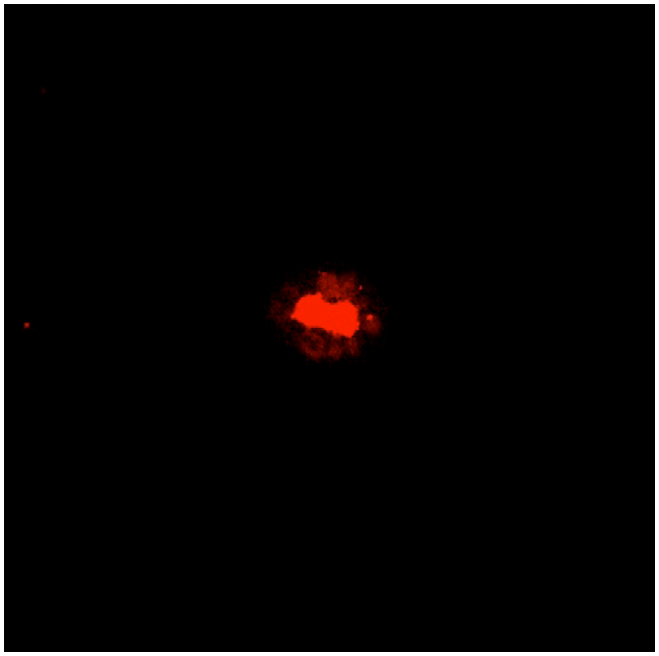

Movie S5. Three-dimensional rotational movie to show distorted F-actin network at the center of the appressorium of the *M. oryzae* Δ*noxR* mutant.

Movie S5

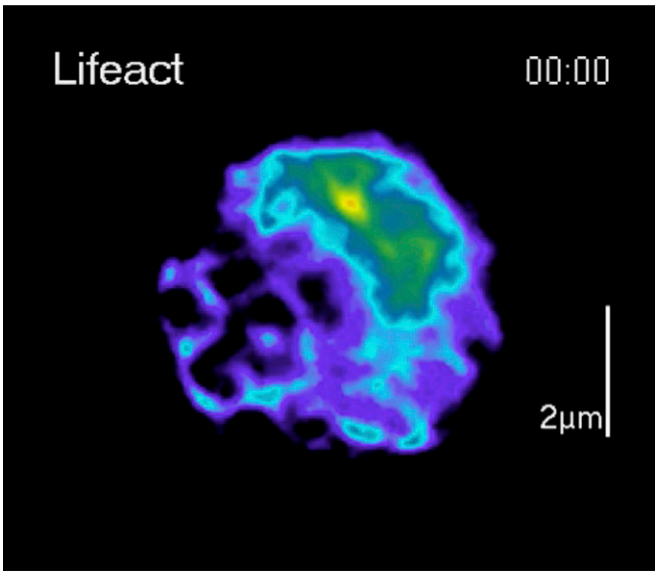

Movie S6. Live-cell imaging to show recovery of LifeAct-RFP after partial photobleaching.

Movie S6

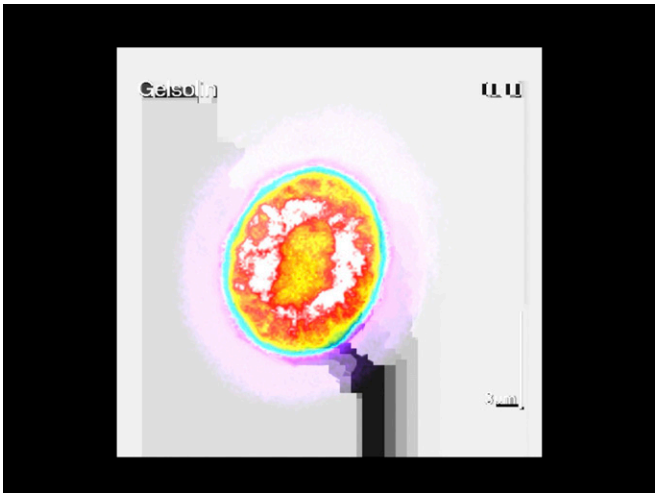

Movie S7. Live-cell imaging to show recovery of Gelsolin-GFP after partial photobleaching.

Movie S7